Modelling SiO_2 solubility over wide *P-T* conditions: advances and open problems

Andrea Maffeis[1]

[1] Università di Torino, via Valperga Caluso 35, Torino (10126), TO.

AM, 0000-0001-9179-1730.

Rend. Online Soc. Geol. It., Vol. 60 (2023), pp. 98-111, 6 figs., https://doi.org/10.3301/ROL.2023.36

Article

Corresponding author e-mail: andrea.maffeis@unito.it

Citation: Maffeis A. (2023) - Modelling SiO_2 solubility over wide *P-T* conditions: advances and open problems. Rend. Online Soc. Geol. It., 60, 98-111, https://doi.org/10.3301/ROL.2023.36.

Associate Editor: Martina Casalini

Submitted: 23 November 2022

Accepted: 12 April 2023

Published online: 26 April 2023

SOCIETÀ GEOLOGICA ITALIANA
FONDATA NEL 1881 - ENTE MORALE R. D. 17 OTTOBRE 1885

ABSTRACT

Fluids in the Earth's crust and upper mantle constantly change chemically, physically, and catalyze different processes, such as mass transfer, with implications for large-scale geodynamics. Silica solubilization has profound implications for mass transfer over a wide range of geologic environments, from upper crustal levels down to the deepest portion of subducting slabs and at the hot base of large orogens. Here I investigate, by using electrolytic fluid thermodynamic modelling, the solubility and speciation of SiO_2 in H_2O at 100–1400 °C and 0–10 GPa, with a particular focus on the geothermal gradients typical in subduction zones and collisional orogens. I show how SiO_2 solubility strongly increases with temperature, reaching dissolved loads between 5 wt% and >70 wt%, within subducting slabs. Results indicate that fluids with dissolved SiO_2 ranging from 3 to 57 wt% along Barrovian and Buchan-type P-T gradients, strongly question the long-standing assumption of the isochemical nature of regional metamorphism. A by-product of this investigation is the tracking of the source of mineralizing fluids responsible for widespread quartz veins back to the deeper and hotter roots of orogens where amphibolitic to granulitic-facies conditions are encountered.

KEY-WORDS: SiO_2 solubility, electrolytic fluid thermodynamic modelling, fluid speciation, mineral dissolution, subduction.

INTRODUCTION

Aqueous fluids are the *sine qua non* gear enabling effective mass and energy transfer across Earth systems, from deep mantle to the surface. Fluids can dissolve and precipitate minerals into the interacting rock, transporting solutes and heat and exchanging components, overall catalyzing deformation via reaction-induced weakening mechanisms. These fluid-involving processes are fundamental because they enable geologic processes like ore deposit formation, long-term chemical cycles at convergent margins or facilitating shear zone development (Goncalves et al., 2012; Tursi, 2022). Ultimately, "aqueous fluids make things happen inside the Earth" (Thompson, 2010; Steele-MacInnis & Manning, 2020).

Background on geologic fluids over wide PT conditions

From low pressure-low temperature (L*P*-L*T*) to ultra-high pressure/ultra-high temperature (UH*P*-HT/UH*T*) metamorphic conditions, fluid chemistry changes during dissolution-precipitation with respect to the *P-T* conditions and rock composition; this becomes especially important with increasing amounts of H_2O-bearing fluid isfreed from minerals through devolatilization reactions; Fig. 1a), leading to five major types of aqueous fluids (Figs. 1a, b):

1) Aqueous fluids with polar gasses: are dominated by H_2O with N_2, which can be complemented by CO_2 or CH_4. These gasses can reach up to 10-15 wt% of components in addition to H_2O (Scambelluri & Phillipots, 2001; Touret & Frezzotti, 2003; Yardley & Bodnar, 2014; Frezzotti & Ferrando, 2015; Manning & Frezzotti, 2020).
2) Brines: contain less than 30 wt% of solutes and are mainly composed of dissolved Na-K-Ca-Mg chlorides (Philippot and Selverstone 1991; Selverstone et al. 1992; Philippot et al. 1995; Scambelluri et al. 2001; Yardley & Bodnar, 2014; Frezzotti & Ferrando, 2015 and references therein; Groppo et al., 2022).
3) Solute-bearing aqueous fluids: have negligible quantities of non-polar gasses together with appreciable amounts of non-

volatile elements (e.g., Si, Al, Ca, Mg, Fe, K, Na, Cl), dissolved as non-volatiles neutral and ionic species bounded to S-Cl-Si-C ligands (i.e., SO_4^-, HCO_3^-, CO_3^{2-}; $HSiO_3^-$, Cl^-), functional groups (e.g., $CHOO^-$) and also possibly containing hydrocarbons (i.e., CH_4, C_3H_8, etc.). Here dissolved Cl is a minor component (Phillippot & Selverstone, 1991; Frezzotti et al., 2011; Sanchez-Valle, 2013; Frezzotti & Ferrando, 2015; Sverjensky et al., 2015, 2019; Guild & Shock, 2020; Li, 2017; Maffeis et al., 2021). They should be characterized by a maximum of 40 wt% of dissolved rock components, however, as with the next major fluid type, no hard upper boundary can be set.

4) Supercritical fluids: from fluid inclusions and multiphase-solid inclusions (also supported by experiments) from UHP rocks (e.g., Ferrando et al., 2005, 2009), characterised by roughly 40 to 60 wt% of dissolved rock components (Manning, 2004a; Kessel et al., 2005; Malaspina et al., 2006; Frezzotti et al., 2007;

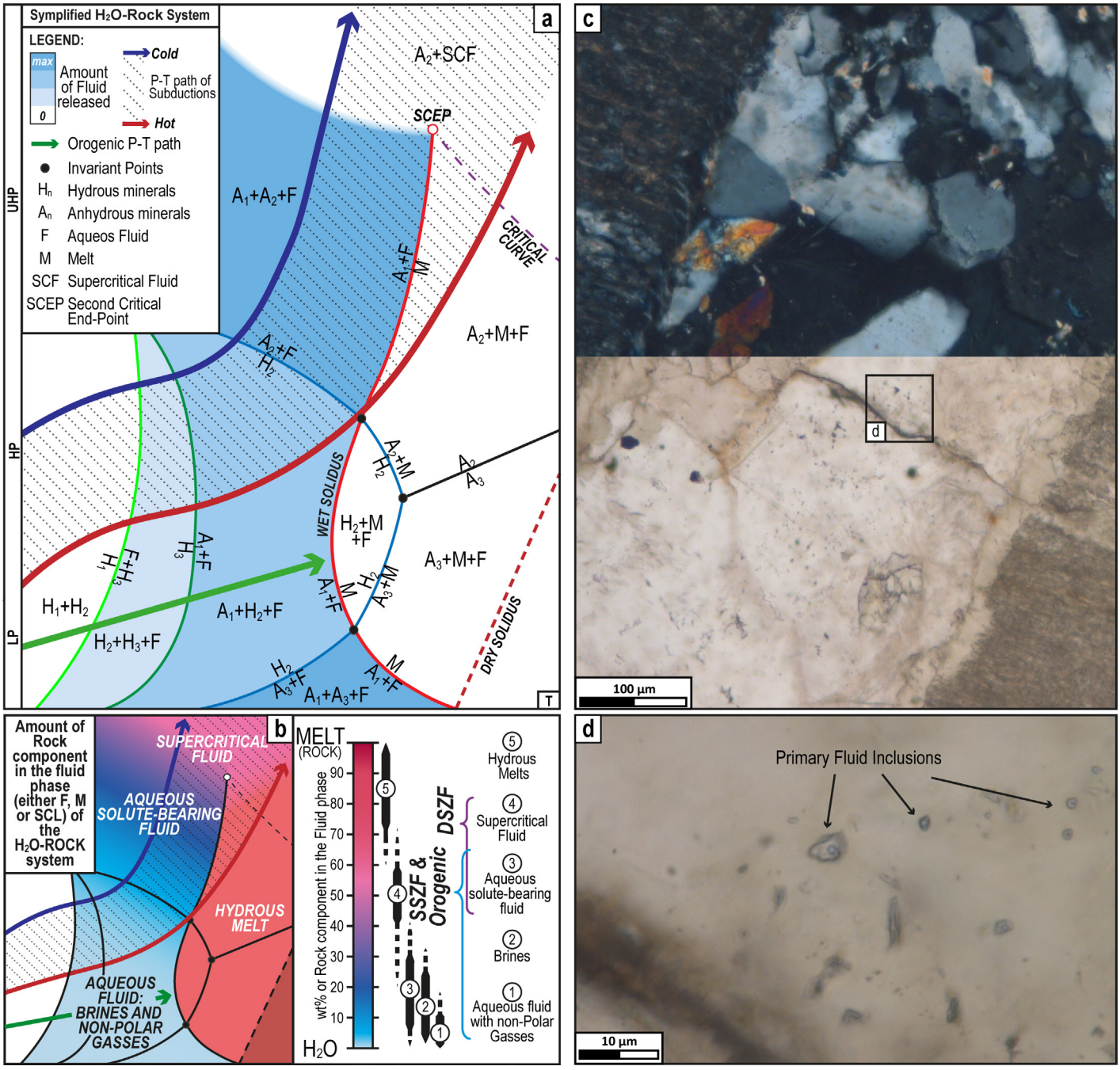

Fig. 1 - a) Idealised topology of phase diagrams characterising subducted and regionally metamorphosed lithotypes, where various dehydration reactions progressively release more and more H_2O in the system (shades of light blue). These reactions lead to the introduction of enough fluid that the solidus is depressed, and, in the hottest subduction zones or in the deepest portion of orogens, the wet solidus can be crossed. Moreover, it also shows how the wet solidus can culminate in the second critical endpoint (SCEP; Ricci, 1951; Manning, 2004a). b) The idealised shift of the dissolved rock component within an aqueous fluid for the same idealised phase diagram in "a". The meaning of the colour coding is reported in the bottom part of the image. SSZF = Shallow Subduction-Zone Fluids; DSZF = Deep Subduction Zone Fluids. c) Photomicrograph of a quartz vein cross-cutting the foliation of a low-grade pelite (Monti Mauri, sample courtesy of Alessandro Petroccia). d) Primary fluid inclusions trapped within the quartz vein shown in c.

Ferrando et al., 2009; Frezzotti & Ferrando, 2015; Ferrando et al., 2019). They are stable above the termination of the wet solidus of the rock system, called the Second Critical End-Point (SCEP; e.g., Ricci, 1951; Kennedy et al. 1962), above which they acquire complete miscibility with the fifth major type of geofluid: hydrous melts.

5) Hydrous melts: they are stabilised above the wet solidus of the rock system and can dissolve increasing amounts of H_2O as *P* and marginal *T* increase. They are thought to be able to host up to 30 wt% of dissolved H_2O (Schmidt et al., 2004; Kessel et al., 2005; Hermann et al., 2006; Mysen, 2012; Spandler & Pirard, 2013), meaning that they cover the range with more than 70 wt% of rock components constituting the fluid.

This mutual solubility between H_2O and rock components in each other (Sanchez-Valle, 2013), becomes more and more pronounced as *T* and *P* increase and is at the core of the wide, but continuous, shift in fluid physicochemical characteristics observed in different environments within Earth. Aqueous fluids with non-polar gasses, brines and solute-bearing aqueous fluids are expected to circulate in shallow subduction environments (Shallow Subduction Zone Fluids, SSZF; Manning & Frezzotti, 2020). Supercritical fluids, hydrous melts, and again solute-bearing aqueous fluids (Deep Subduction Zone Fluids, DSZF; Manning & Frezzotti, 2020) are expected to be stable in the deeper portions of a subducting slab, transitioning from one to another depending on the slab temperature or proximity to the overlying mantle wedge. Finally, orogenic wedges are expected to be permeated by aqueous fluids with non-polar gasses, brines and, in their roots, by hydrous melts.

Importance of the SiO_2-H_2O system and scope of this work

This continuous spectrum of geologic fluids can be investigated directly, through fluid inclusion studies or experimental petrology, or indirectly, by thermodynamic modelling. The latter, in the last 10 years, has seen relevant advancements in its capabilities both with available thermodynamic databases (Deep Earth Water model, Sverjensky et al., 2014) and with algorithms able to deal with complex fluids such as solute-bearing aqueous fluids (Galvez et al., 2015; Connolly & Galvez, 2018). It is now possible to routinely model electrolytic fluids in addition to classical molecular fluids.

Silicon is one of the most abundant and also one of the most soluble rock-forming elements composing Earth's lithosphere and one of the few for which extensive experiments have been conducted (Manning, 2018). Thus understanding SiO_2 dissolution behaviour can shed light on the potential mass-mobilising capacity of geologic fluids and allows to examine their constantly changing nature over a wide range of *P*–*T* conditions. As recently reviewed by Manning (2018), silica solubility in H_2O rises from its ability to polymerise. Experiments have shown that the most common dissolved silica specie is the monomeric orthosilicic acid (H_4SiO_4, hereafter referred to as silica monomer for simplicity) at lower *T*. However, at higher *P* and *T* such monomers combine with each other by sharing one bridging oxygen, thus producing silica dimers ($H_6Si_2O_7$). However, above 800°C predictions based solely on these species fail to reproduce the higher dissolved silica concentration measured in experiments. As envisioned by Newton & Manning (2008), silica species with higher polymerisation degrees have been invoked to account for the underprediction of dissolved silica in fluids at H*T*. From these observations, the latest update of the DEW model (Huang & Sverjensky, 2019) saw the introduction of silica trimers ($H_8Si_3O_{10}$) as a specie with higher polymerisation than silica dimers. In their calibration against mafic eclogitic-derived fluids at UH*P* conditions, such specie was able to reconcile thermodynamic predictions and experimental observations regarding silica solubility at H*T*. However, this hasn't been tested with results from simpler SiO_2-H_2O experiments.

Understanding and modelling silica solubility is also a starting point from which one may observe that solute-bearing aqueous fluids might be more common, throughout Earth's crust, than generally thought. This might help explain the common quartz veins (which can constitute about 1-30 vol% - or even up to 40 vol% - of regionally metamorphosed rocks; Ague, 2014 and references therein) typically precipitated at greenschist faces conditions (Fig. 1c) from fluids rising from deep within orogenic wedges (Fig. 1c). However, real rocks are more chemically complex than a simplistic SiO_2-H_2O system and the combined dissolution behaviour of the major (e.g., Al, Ca, K, Na, Mg, Fe, C, etc.) and minor (S, Ti, Mn, Cr, P, N, etc.) rock-forming elements will result in fluid compositions and speciation that are unique for each rock (assuming, in a further simplifying way, a closed system fluid-rock evolution). Nevertheless, the presented results serve to highlight the possibility that solute-bearing fluids might circulate in deep slabs and orogenic wedges in addition to simpler molecular fluids with polar gasses, brines and melts.

In this contribution, I explore the SiO_2-H_2O system using electrolytic fluid models to model dissolved Si speciation and concentration along typical subduction and orogenic P-T paths. Despite the simple chemical system, this work allows gaining deep insight into the often overlooked potential of fluids to act as effective mass transfer mediums through the crust. By doing this, it is shown that fluids are more complex than routinely envisioned and as such their properties (composition and speciation) can vary by order of magnitude across an orogenic wedge or in a subducting slab.

METHODS

Pressure-temperature (between 100 and 1400°C and between 0 and 10 GPa) isochemical phase diagrams (Fig. 2) have been calculated by means of the software package Perple_X (version 6.9.1; http://www.perplex.ethz.ch; Connolly, 2005; Connolly & Galvez, 2018) in the SiO_2-H_2O-O_2 chemical system. The phase diagrams were calculated with the "Lagged Speciation" algorithm (i.e., by iteratively refine speciation results by simple back-calculation; Galvez et al., 2015; Connolly & Galvez, 2018) with condensed phase and molecular volatile species data from Holland & Powell (2011 revised 2018, version DS6.33) and solute species data from the DEW/HKF model of Huang & Sverjensky (2019). For these calculations, the solvent consists of a mixture of H_2O, H_2 and O_2. The Pitzer & Sterner (1994) equation of state (EoS)

was used to describe pure H_2O, all other pure fluid properties were computed from the Redlich-Kwong EoS, while the Modified Redlich-Kwong (MRK) EoS of DeSantis et al. (1974) was used to compute the activities of the molecular species in the solvent. To model the fluid solute composition and speciation all fluid species have been considered, except for the corresponding molecular species already accounted for in the solvent (i.e., H_2O, O_2, H_2, H^+, HO_2^-, OH^-, $HSiO_3^-$, H_4SiO_4, $H_6Si_2O_7$, $H_8Si_3O_{10}$). The selected mineral endmembers are all the SiO_2 polymorphs and the used fluid model is COH-Fluid+ (Connolly & Galvez, 2018). The thermodynamic properties of the silica polymorphs are unchanged since Holland & Powell (2011), and since such properties were derived considering also high-pressure experiments, other versions of the database (i.e., DS5.5 and older) were not tested. However, two different melt models, applicable at SiO_2-rich melt compositions and over a wide range of *P* and *T*, have been used and the results compared. They are the melt model of White et al. (2014) and the melt model of Holland et al. (2018), for which only the melted silica end-member differ. To test the impact of higher dissolved silica polymers, calculations with and without silica trimers have been conducted (thermodynamic properties of silica monomers and dimers are unchanged since the first version of the DEW model; Sverjensky et al., 2014). Nevertheless, calculations without silica trimers are used only to benchmark their impact and are not considered representative of the SiO_2-H_2O system.

DATA

The SiO_2-H_2O system

The system has been explored by modelling the dissolution of 20 kg of SiO_2 in 1 kg of H_2O (three-component bulk composition adjusted for excess O_2 in order to stabilize an H_2-free fluid: 332.889 SiO_2 mol, 55.4 H_2O mol and 10^{-6} O_2 mol) in order to push at higher temperatures the complete dissolution of SiO_2 mineral phases. The calculated phase topology of the SiO_2-H_2O system (Fig. 2) reproduces the expected isomorphic phase transition between SiO_2 polymorphs in the SiO_2-H_2O system, as calculated by Hack & Thomson (2011). However, fluid and melt involving phase boundaries, like the wet solidus (pink curve, Fig. 2a) and a supposed complete dissolution of SiO_2 polymorphs into a homogenous fluid phase (a solubility curve, purple curve; Fig. 2a), resulting in a monophase high variance field, are different (the wet solidus) if not unexpected (the solubility curve). A fluid phase where H_2O behaves as the solvent is modelled together with quartz, coesite and stishovite. However, the modelled phase diagram is missing the Upper Critical End Point, which has been experimentally located at 1080°C and 0.95-1.00 GPa (the point at the end of the dashed pink curve, Fig. 2a; Kennedy et al., 1962; Manning, 1994; Newton & Manning, 2008; Hunt & Manning, 2012). The melt models of White et al. (2014) and of Holland et al. (2018) produce two different wet solidus topologies, neither of which fully reproduces the experimentally derived one. Both calculate an arched wet solidus geometry. The White et al. (2014) wet solidus follows the experimental one up to 0.5 GPa and then deviates at higher *T* and at increasing *P*, asymptotically approaching the *P* of the Critical Point (i.e., 0.95-1.00 GPa). This results in a triangular region between, roughly, 1090°C-0.5 GPa, 1080°C-1 GPa and 1200°C-1 GPa where the modelling extends the fluid+quartz field at the expense of the experimentally observed quartz+melt field (the position, in the *P-T* space, of the experiments in the SiO_2-H_2O systems are reported as green circles in Fig. 2a as a reference; Kennedy et al., 1962; Anderson & Burnham, 1965; Manning, 1994; Zotov & Keppler, 2002; Wang et al., 2004; Newton & Manning, 2008; Mysen, 2010; Hunt & Manning, 2012). The Holland et al. (2018) wet solidus, on the other hand, wraps around the PT space of the correct wet solidus, lowering the minimum temperature of melting by a maximum of ~130°C (dotted pink lines in Fig. 2a). Melt-bearing fields are encountered on the high-temperature side of the wet solidus and of the solubility curve and, in all these cases, below 3 Gpa (in the modelled T range; Fig. 2a).

Fluid chemistry

As shown in Fig. 2, SiO_2 (as wt%) isopleths in the fluid phase visualise the continuum increase in silica solubility in H_2O as pressure and temperature increase. Above roughly 0.5 Gpa, the slope of the isopleths changes based on the silica polymorph that is dissolving in the fluid (Fig. 2). From the top of the diagram, when stishovite is dissolving, SiO_2 isopleths are characterised by a positive slope. In the coesite stability field, the isopleths slope is still positive but nearly vertical with respect to those in the stishovite stability field (Fig. 2). Finally, in the quartz stability field, the isopleths show a negative slope that, at low pressure, changes and becomes nearly horizontal. The pressure at which the isopleths inflexion (in the quartz-stability field) is located increases with temperature, from roughly 0.1 GPa at 350°C to 0.25 GPa at 600°C, and around 0.4 GPa at 900°C (Fig. 2c). Such topology leads to an abrupt change in SiO_2 solubility between 500°C and 1100°C and below 0.2 GPa: a decrease by an order of magnitude from 1 wt% down to 0.1 wt% at 0.1 GPa. Below 0.1 GPa, the 0 wt% isopleth marks the lower stability field of liquid H_2O, indicating the presence of a *P-T* region where vapour is stable. Here, for vapour-like fluids, the Helgeson-Kirkham-Flowers formalism (i.e., the equation of state on which electrolytic fluid thermodynamic modelling is based on the Lagged speciation algorithm, Galvez et al., 2015; Connolly & Galvez, 2018) is not fully parametrised and does not extrapolate plausibly (Shock et al., 1992; Connolly & Galvez, 2018). For this reason, these shallow *P-T* conditions, more relevant for superficial hydrothermalism, will not be dealt with. Generalising, the slope of silica solubility shown in Fig. 2 is strongly *T*-dependent in the coesite stability field and in the upper portion of the quartz stability field, while in the stishovite stability field and in the lower portion of the quartz stability field *P* plays also a significant role. More specifically, silica solubility increases by one order of magnitude from <0.1 wt% to 1 wt% between ~250-350 °C and 450-500 °C and then reaches 10 wt% between ~750 °C and ~850 °C in the upper portion of the quartz stability field and coesite stability field. Above 850°C, SiO_2 solubility increases dramatically until the complete solubilization of silica into the fluid, which is modelled to occur above 1200°C

for coesite and between 1200 and 1400 °C for quartz (Fig. 2). On the other hand, *P* has opposite effects in the stishovite stability field and in the lower part of the quartz stability field. The positive slope of dissolved SiO_2 isopleths in the stishovite stability field predicts a decrease in silica solubility as *P* continue to increase, at constant *T*, above 6-9 GPa. On the other hand, SiO_2 solubility increases with increasing *P*, by up to two orders of magnitude, between 0 and 0.2 GPa (Fig. 2).

DISCUSSION

Experimentally determined vs thermodynamically modelled SiO_2-H_2O phase diagram and SiO_2 solubilities

Two topological characteristics of the calculated phase diagram and the SiO_2 isopleths show some mismatch with previous works (Fig. 2a). The first is the wet solidus. Two melt models have been tested: the White et al. (2014) and the Holland et al. (2018) models.

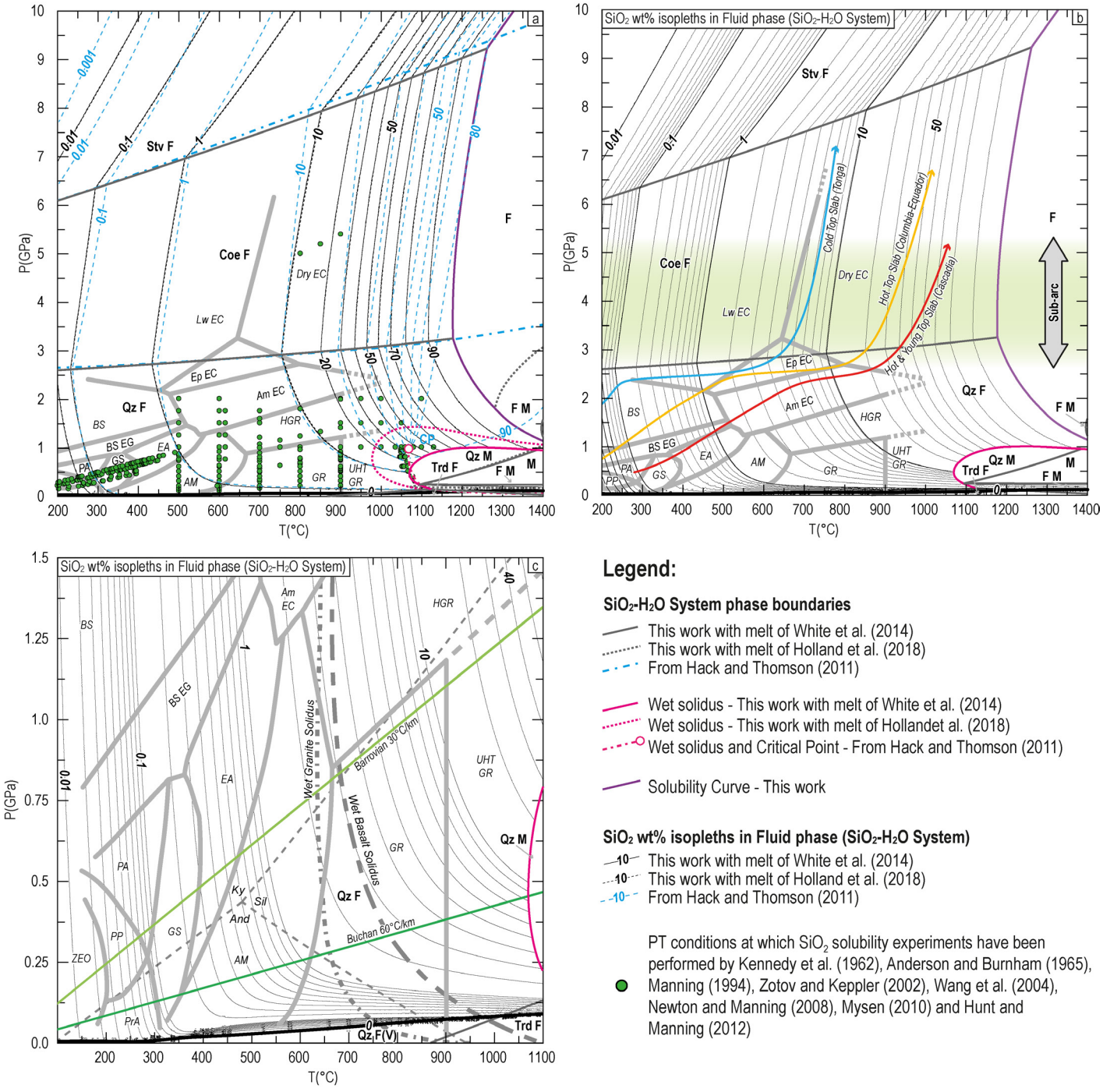

Fig. 2 - Topology of the calculated isochemical phase diagram of the simple SiO_2-H_2O chemical system, where dissolved SiO_2 isopleths in the fluid are reported. a) The dashed light blue lines are phase boundaries and SiO_2 isopleths within the fluid calculated by Hack & Thomson (2011), as well the true wet solidus with its critical point (CP; these have been drawn from Kennedy et al., 1962). The experimental data have been compiled from: Kennedy et al. (1962), Anderson & Burnham (1965), Manning (1994), Zotov & Keppler (2002), Wang et al. (2004), Newton & Manning (2008), Mysen (2010) and Hunt & Manning (2012). b) Subduction P-T paths are from Syracuse et al. (2010), and the sub-arc P range is from Hermann & Spandler (2008). c) The granite wet solidus is from Makhluf et al. (2017), while the wet basalt solidus is from Schmidt & Poli (1998).

The first is calibrated for silica-rich pelitic systems, while the other is a more generalist model that should be able to produce melting relations over a wide range of compositions (i.e., from ultramafic to basaltic, to tonalitic, to pelitic, to granitic compositions). Among the two, the White et al. (2014) model, below 0.5 GPa, reproduces the experimental wet solidus, while above it departs significantly. However, such results are still preferable to those of Holland & Powell (2018), which result in a significant expansion of the melt-bearing field at lower *T* and higher *P*. This might indicate that the Holland & Powell (2018) melt model, although it is more complex than the model the one of White et al. (2014), is more sensible of the activity of other melt components. For this reason, from here forward, the calculation with the White et al. (2014) model will be used as the reference model (Fig. 2b, c). Even though different melt models have no impact on the SiO_2 isopleths, especially close to the wet solidi (Fig. 2a), the second topological mismatch is the isopleths of dissolved SiO_2 above 850 °C and specifically around where the critical point should be (Fig. 2a). The light blue dashed isopleths in Fig. 2a have been calculated by Hack & Thomson (2011) up to 900°C and 2.5 GPa (based on Manning, 1994) and then extrapolated at higher *T* based on experimental constraints available at the time. The 2019 update of the DEW model (Huang & Sverjensky, 2019) added new hydrous silica species (silica trimers, see later) that changed modelled silica solubility at higher *T*. In the coesite and stishovite stability fields, silica solubility isopleths modelled in this work are topologically sound and match the progressive increase observed at lower temperatures. However, in the quartz stability field, the arched geometry of the wet solidus and the lack of the upper second critical endpoint strongly alters the isopleth topology. The isopleth marking 10 wt% of dissolved silica is the one (moving from low to high temperature) matching the results of Hack & Thomson (2011). Following the theoretical treatment of Hack et al. (2007) phase diagram topology around critical points (on which the Hack & Thomson (2011) phase diagram has been drawn), modelled silica solubility isopleths in the quartz stability field (i.e., between 1 and 2.5 GPa above 1000 °C) are not correct.

When comparing experimental and modelled solubilities (Kennedy et al., 1692; Anderson & Burnham, 1965; Manning, 1994; Zotov & Keppler, 2002; Wang et al., 2004; Newton & Manning, 2008; Mysen, 2010; Hunt & Manning, 2012) a more complete picture emerges (Fig. 3). Experimental silica solubilities at greenschist facies conditions and below are low (up to ~0.5 wt%) and slightly under-estimated by thermodynamic modelling, which predicts solubilities close to a 1:1 ratio, but slightly lower and reaching up to ~0.4 wt% (Fig. 3a). At amphibolitic facies conditions, experimental silica solubilities range from 0.2 to 2 wt%, while thermodynamic one range from 0.3 to 2 wt%, with experimental solubilities above 0.7 wt% that are accurately reproduced (Fig. 3c). Of the very few experiments at H*P* and UH*P* conditions (Fig. 3b), only the three experiments at 5-5.4 GPa of Mysen (2010) differ significantly. As already noted by Manning (2018) the experiments of Mysen (2010) behave differently from all the other experimental studies on the system and as such, they will not be considered. Thus, at HP conditions, experiments and thermodynamic modelling both agree and produce fluids with 1-6 wt% of dissolved SiO_2 (Fig. 3b). At H*T* and UH*T* conditions (i.e., at granulitic facies conditions and above) experiments and thermodynamic modelling suggest that SiO_2 solubility can range as little as 0.4 wt% up to 80 wt% (Fig. 3e, g, i). Thermodynamics and experiments roughly agree with the general increase in SiO_2 solubility as T increases, but thermodynamics seem to under-estimate by roughly 1-10 wt% above 800°C and 20 wt% of dissolved load (Fig. 3i, m). Additionally, a group of experiments are strongly under-estimated by modelling, with a mismatch that ranges between 10.5 and 50 wt% (Fig. 3i, m): these are experiments located around the critical point and in the triangle between roughly 1090°C-0.5 GPa, 1080°C-1 GPa and 1200°C-1 GPa. Here the melt-bearing side of the experimental wet solidus of the system is substituted, in the modelling, by a fluid + quartz field. This results in an artificial underestimation due to the inaccuracy of the melt model rather than that of the fluid model.

The importance of the silica trimers in modelling SiO_2 solubility is highlighted in Fig. 3c, f, h, l and m. Here is readily observable the strong and systematic under-estimation that thermodynamic modelling incurs above 5-10 wt% of dissolved SiO_2 and above 800-850°C. Experimental solubilities can be under-predicted by 10 to even 60 wt%. This was already observed by Manning (2018), but, as he had foreseen, considering silica trimers in the calculations allows to strongly reduce such errors. This mismatch is further enlarged for those experiments around the critical point, whose underestimation ranges between 20 and 90 wt% of dissolved silica.

Overall, electrolytic fluid thermodynamic modelling that uses the latest version of the DEW database (i.e., including silica trimers in the calculations), is capable of reliably reproducing solubility experiments up to 20 wt% and between 20 and 80 wt% with an average underestimation up to 10 wt%. Three reasons might be responsible for the discrepancy at high dissolved loads: (i) error in thermodynamic properties of dissolved silica species, (ii) topological errors deriving from the inability of the modelling to correctly account for the critical behaviour of the system or (iii) an undiscovered highly polymerised silica specie(s) stable above 800°C. All these reasons are not mutually excluding and may combine, leading to the observed discrepancies. However, a deeper understanding of the major source of error in the presented calculations is out of the scope of this work. Nevertheless, the relevance of such errors is diminished by the fact that this region in the *P-T* space is more likely to be at super-solidus conditions for most common crustal rocks, or not even existing since these are *P-T* conditions typical for the upper lithospheric mantle in the case of a thinned crust.

Silica solubility as a function of geodynamic regime

Comparing the fluid bulk composition at conditions typical of the top of a subducting slab, in the range from cold to hot and young slabs of Syracuse et al., 2010 (Fig. 2b), and also between them and classical regional metamorphism *P-T* gradients (i.e., Barrovian and Buchan type, with geothermal gradients of 30°C/km and 60°C/km, respectively, e.g., Copley & Weller, 2022; Fig. 2c), quite relevant differences emerge (Fig. 4a, c).

Subduction Zones

The coldest slab tops, at sub-arc depths (roughly between 2.75 and 5 GPa; Hermann & Spandler, 2008), are characterized by a *P-T*

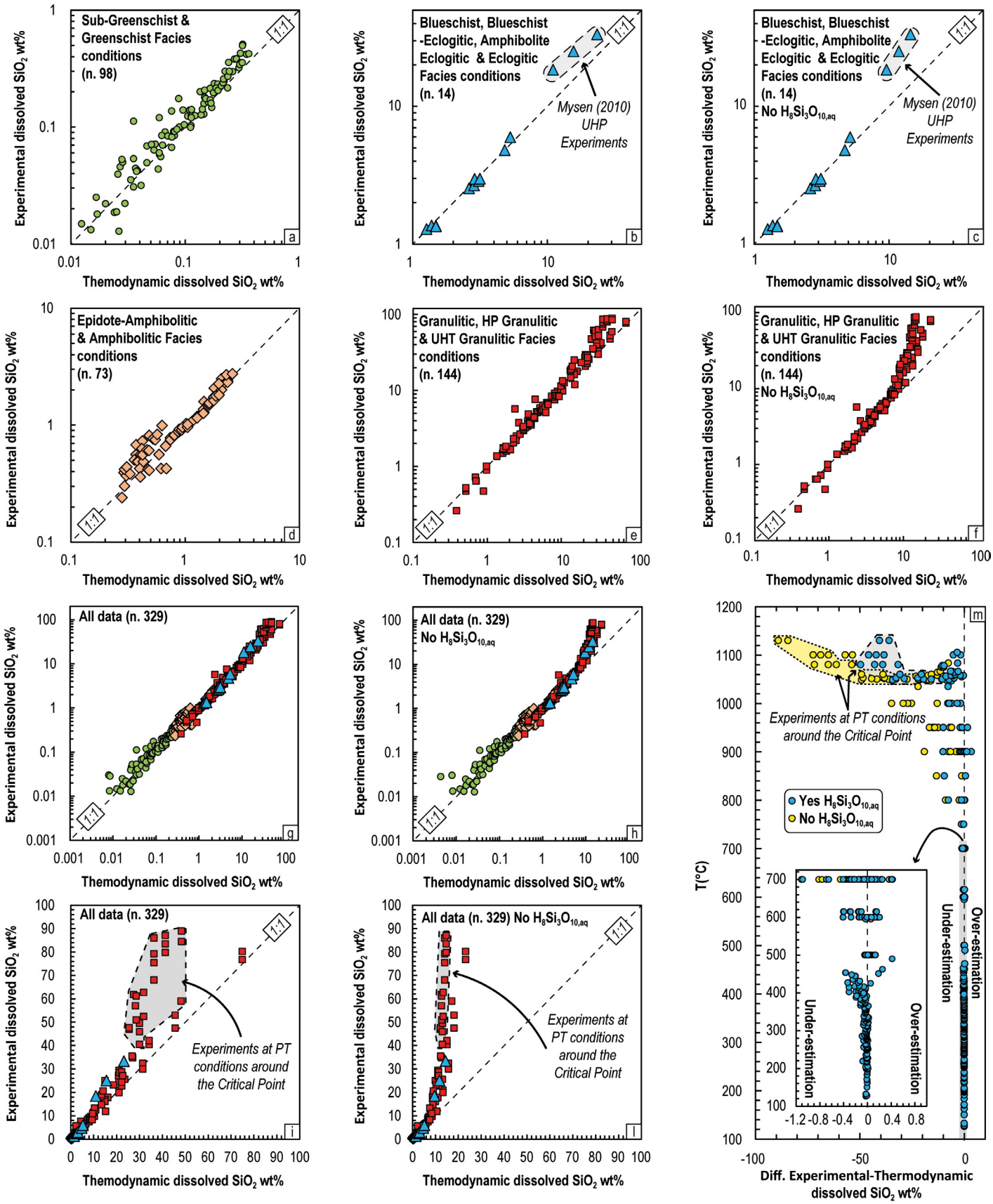

Fig. 3 - a-l) Comparison between experimental and thermodynamic modelled silica solubilities at varios PT conditions and with different modelling setups. a, b, d, c) Comparison for the reference modelling with silica trimers included. c, f) Comparison with silica trimers excluded from the calculation. Results at greenschist and amphibolitic facies conditions are identical to those obtained with silica trimers included in the calculations: they are identical to a and d and as such have not been shown. g, h) Entire range of comparison between experimental and thermodynamically modelled silica solubility in bilogaritmic plots, in (h) are shown results without silica trimers. i, l) Same plots in g and h as simple linear plots, allowing to enhance deviation at high dissolved load. m) Difference between experimental and thermodynamic silica dissolved load as a function of T.

gradient that, in the *P-T* space, is parallel to the SiO_2 isopleth of 7 wt% (Fig. 2b). This means that, in the coldest slabs, above 4 GPa H_2O is unable to further mobilising any other SiO_2 and thus mineral dissolution effectively stops in the SiO_2-H_2O system. This explains the lack of increase and even the slight decrease in dissolved silica shown in Fig. 4a for a cold slab (light-blue curve). Fluids with such dissolved load are solute-bearing aqueous fluids, albeit relegated to the lower end of the spectrum. Hot slabs (yellow curve in Fig. 4a) follow the same silica increase path with increasing *T*, despite being at lower *P*. This is allowed by the negative slope of the dissolved silica isopleths (Fig. 2b). At the fore-arc to sub-arc transition, aqueous fluids in a hot slab can dissolve up to 12 wt% of silica, and at sub-arc depths this increases dramatically, reaching up to ~35 wt% of dissolved silica. This value is in the upper end of what can be considered a solute-bearing aqueous fluid and might even be considered (only from the solute load point of view) a diluted supercritical fluid. However, the *P-T* conditions of a hot slab at sub-arc depths (i.e., 850-950 °C and 2.75-5 GPa, Fig. 2b) are quite far away from those expected to be above the second critical endpoint of the SiO_2-H_2O system (between ~1000 °C and ~1200 °C and above 0.95-1.00 GPa, Kennedy et al., 1962; Manning, 1994; Newton & Manning, 2008; Hunt & Manning, 2012). This means that such fluid is not necessarily in a supercritical state. Finally, the hottest slabs (i.e., the youngest) reach the fore-arc to sub-arc transition with rather high dissolved loads of ~28 wt% and seem to be able to reach extremely high dissolved loads of ~75 wt%. This range of compositions is more akin to a proper supercritical fluid (allowed by the temperature range greater than 900 °C, Fig. 4a), if not an H_2O-rich hydrous melt in the deepest portion of the slab. However, as shown above, the reliability of the modelled solubilities can be affected by a minimum error of 10 wt%. This makes classifying a modelled fluid with up to 75 wt% of dissolved rock components as a hydrous melt somewhat problematic. The latest thermodynamic properties of dissolved silica species in the coesite stability field are derived by H*P*-UH*P* experiment with a mafic system (Kessel et al., 2005; Dvir et al., 2011; Huang and Sverjensky, 2019), thus a direct comparison between modelled data and these experiments is not possible. Nevertheless, mass transfer by dissolution in the subducting slab (e.g., Manning, 2004; Herman et al., 2006; Frezzotti et al., 2011; Ferrando et al., 2017; Maffeis et al., 2021) is a petrologic process that has the potential to drastically change the chemical composition of both the source rocks and of the rocks in which such fluids will infiltrate as they rise due to buoyancy (Hack & Thomson, 2011). An example of such metasomatic interaction, between silica-rich fluids and mantle peridotites, are the orogenic garnet-orthopyroxenites found at the slab-mantle interface and formed at sub-arc depths (e.g., Malaspina et al., 2006).

Orogenic Wedges

At more classically investigated Barrovian and Buchan *P-T* conditions, fluids are thought and modelled either as aqueous fluids with non-polar gasses dissolved in them or as brines (e.g., Yardley & Graham, 2002, Steele-MacInnis & Manning, 2020), with the latter capable of carrying up to 30 wt% of dissolved Cl-complexed solutes (Yardely & Graham, 2002). However, experiments (see Fig. 2a) and thermodynamic models capable of treating electrolytic fluid chemistry suggest that another type of fluid is potentially stable: Cl-free solute-bearing aqueous fluids. Along a Barrovian type *P-T* gradient of 30 °C/km, fluids can carry more than 1 wt% of dissolved silica only above ~520 °C (at ~0.6 GPa; Fig. 2c, 4a, c): at amphibolite-facies conditions. On the other hand, along a Buchan-type gradient of 60 °C/km, such capability is reached at higher temperatures: close to granulite-facies conditions at ~600 °C (at ~0.25 GPa; Fig. 2c, 4a, c). The granite and basalt wet solidi (relevant for pelitic and quartz-feldspatic systems) are located between 650 °C and 700 °C and between 700 °C and 800°C along Barrovian and Buchan gradient, respectively (e.g., Schmidt & Poli, 1998; Makhlul et al., 2017). This means that at granulite-facies conditions, aqueous fluids are more likely to trigger partial melting and complete dehydration of the system than to reach solubility capability higher than 2-3 wt% of dissolved silica (Fig. 2c, 4a, c). However, if the system has already experienced some melt extraction (e.g., Groppo et al., 2012) or if the solidus of the system is located at high temperatures, external (i.e., relative to any considered rock volume at depth) aqueous fluids might find them self undersaturated in silica: at these conditions (e.g., above 800°C) silica saturation in the fluid ranges from (i) 3 to 9 wt% along Buchan-type gradient and (ii) from 7 wt% to 57 wt% at 1100°C along Barrovian-type gradient (Fig. 2c). This might lead to (extensive) quartz dissolution or even a reaction between a silica-undersaturated fluid and the silicate mineral assemblage, leading to the stabilization of a fluid that, potentially, can transport between 1 and 10 wt% of dissolved silica at granulite-facies conditions (i.e., up to 900°C; Fig. 2c, 4a, c).

Silica speciation: probing the fluid-structure

As shown above, silica solubility increases as pressure and, most importantly, temperature increase (Fig 2, 4a, b), but how? As pressure and temperature increase, the structure of the water molecule changes as well. This is expressed with the dielectric constant of water, which is a measure of the polarization degree of the H_2O molecule and, thus, of the capability of H_2O to form solvation shells around dissolved ions (e.g., Sverjensky, 1987). However, the dielectric constant of water increases with pressure and decreases with temperature. These changes, combined, lead to a general decrease of the H_2O dielectric constant from H*P* to UH*P* conditions and beyond. While leading to a weaker solvation capacity of H_2O, the lowering of the dielectric constant in turn favours changes in the solute structure, leading to the complexation of oppositely charged ions (Sverjensky, 2019). The resulting complexes will become bigger and progressively more polymerised (i.e., more complex molecules; Fig. 5) as the system progresses toward greater pressures and especially temperatures (e.g., Sanchez-Valle, 2013). The described change in the dielectric constant of H_2O is the reason for the increased solubility of rock components within H_2O at UH*P* and H*T* conditions (Sverjensky, 2019).

In the modelled fluid, dissolved silica speciation and polymerisation change in a similar way at different pressures as temperature increases (i.e., along different *P-T* paths; Fig. 4c, d)

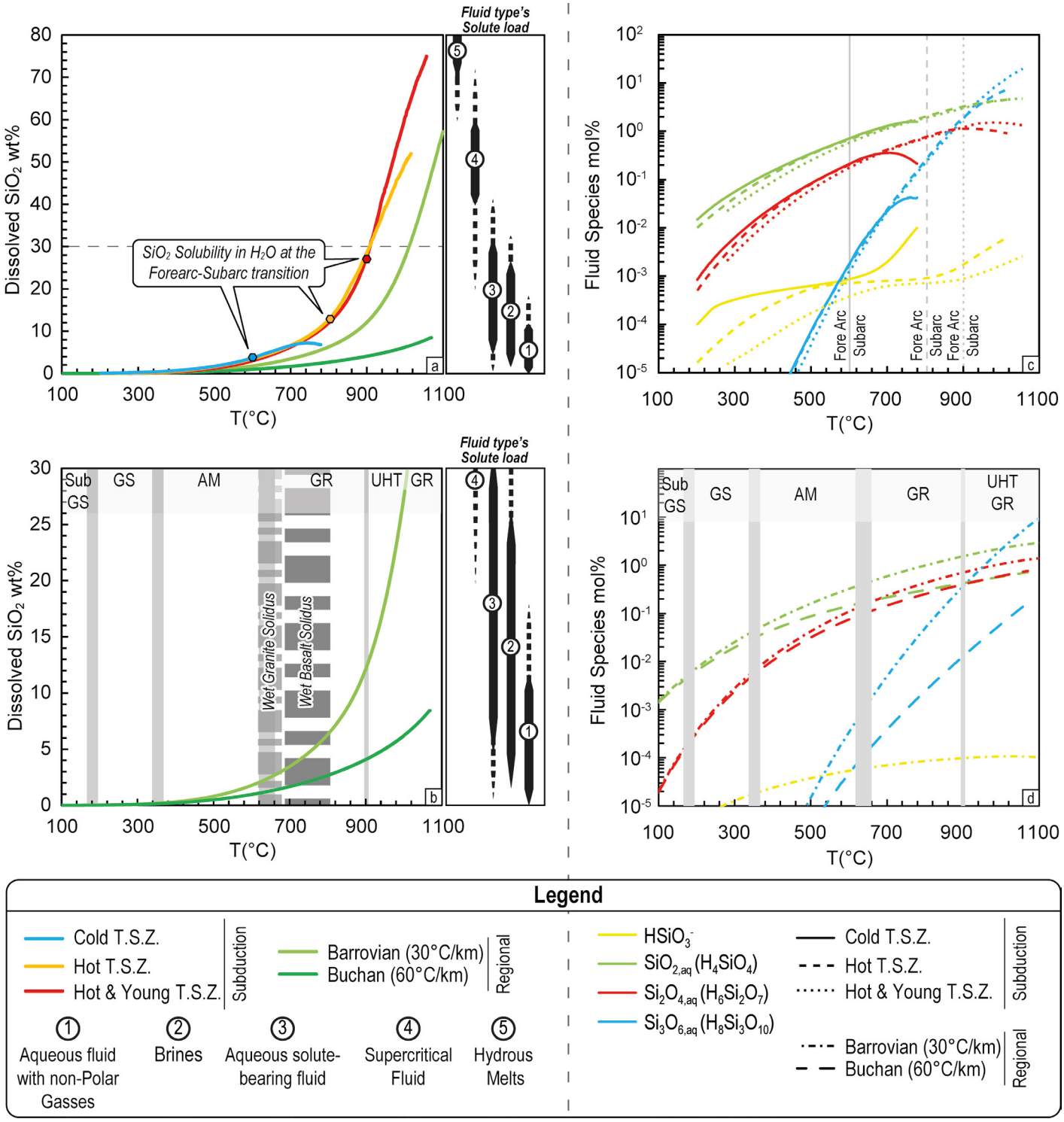

Fig. 4 - a) Dissolved SiO_2 as wt% across different P-T paths, with the transition from fore-arc to sub-arc depths marked by hexagons for the subduction P-T paths. b) Same as in (a), but only for orogenic P-T pathsand with the metamorphic facies highlighted. c, d) Silica speciation along different P-T paths.

due to the stronger dependence of silica solubility on temperature rather than the pressure in both quartz and coesite stability field (Fig. 2). Along subduction *P-T* paths, silica monomers ($H_4SiO_{4,aq}$, also written as $SiO_{2,aq}$) dominate fluid speciation up until 900 °C (i.e., increasing from 10^{-2} up to 4 mol%; Fig. 4c), while along orogenic regional geotherms it retains its dominance (i.e., increasing from 10^{-3} up to 1 mol%; Fig.3d). Silica dimers ($H_6Si_2O_{7,aq}$, also written as $Si_2O_{4,aq}$) are roughly less abundant by one order of magnitude than silica monomers, but at subarc and at granulite-facies conditions they reach similar concentration to those of silica monomers (i.e., increasing from 10^{-3} up to 1 mol%; Fig. 4b, d). The silicate anions ($HSiO_3^-$) is the third specie by abundance, although with quite low concentrations until 520-580 °C (i.e., $<5*10^{-4}$ mol%), where silicate trimers ($H_8Si_3O_{10,aq}$, also written as $Si_3O_{6,aq}$) rapidly (i.e., within a few hundreds of degrees) rise and surpass them. Silica trimers reach and exceed silica dimers and silica monomers between ~850 °C

and ~900 °C, respectively, along subduction *P-T* paths. On the contrary, silica trimers are able to surpass only silica dimers at UH*T* granulite-facies conditions along Barrovian-type geotherms. Along Buchan-type geotherms they remain one order of magnitude less concentrated than both silica dimers and monomers (Fig. 4d). Overall, silica trimers show an increase in abundance between four and five orders of magnitude at *P-T* conditions typical of regional metamorphism, while they can experience an even more significant increase of more than six orders of magnitude (from < 10^{-5} mol% up to 20 mol%) in the hottest slabs. The appearance of silica trimers, and the increase in abundance of silica dimers, corresponds to the expected increase in the polymerisation of dissolved silica in the fluid as *P* and *T* increase (Fig. 5).

The modelled change in fluid structure, exemplified by the increasingly more complex (Fig. 5) and abundant dissolved silica species, has important implications for mass transfer efficiency and other physical properties of geologic fluids. At sub-arc depths, fluids dominated by silica trimers and with a dissolved load ranging from 40 to 70 wt% might be considered supercritical liquid with a structure that is more akin to that of a hydrous melt (Fig. 4, 5; Manning, 2004a). A polymer-bearing fluid (either a solute-bearing aqueous fluid or a supercritical fluid) will display different viscosity (Hack and Thomson, 2011, continuous shift from aqueous fluid-like to melt-like viscosities) and diffusivity than a simpler electrolyte solution (i.e., a brine; Manning, 2004b). Metasomatic interaction between subduction-zones fluids, with different degrees of silica polymerisation, and the overlying mantle wedge might require a different amount of fluid to obtain the same results (i.e., differences in chemical potential between different fluids with different polymerization degrees; Newton & Manning, 2003; Manning, 2004b).

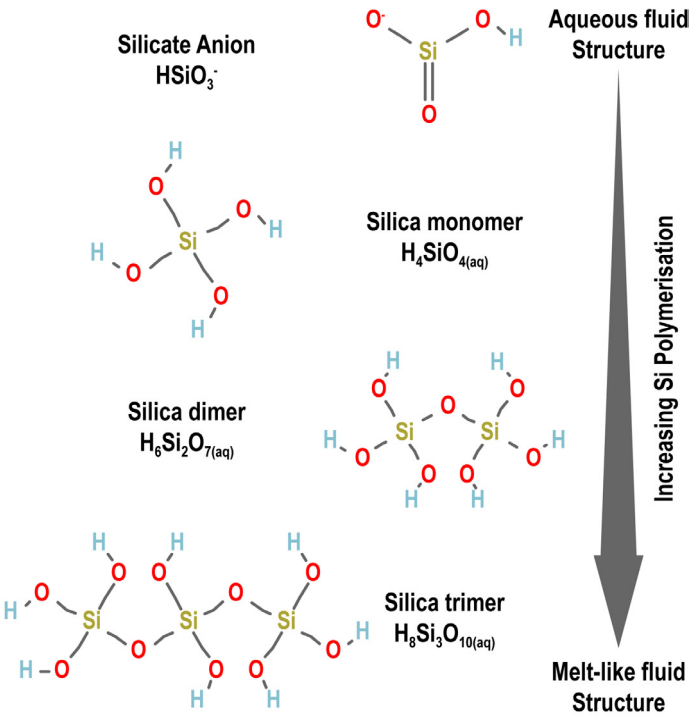

Fig. 5 - Structural formulae of the silica species modelled in this work (structures redrawn from PubChem).

Field evidences: quartz veins

The fact that mineral dissolution and associated mass transfer can occur in a subducting slab has been proven in multiple experimental, thermodynamic and natural evidence throughout the last 20 years (e.g., Kessel et al., 2005; Hermann et al., 2006; Malaspina et al., 2006; Frezzotti & Ferrando, 2015; Maffeis et al., 2021). However, the possibility that major rock-forming elements might be mobilised during regional metamorphism is an idea that has been debated since the first half of 20th century (e.g., Shaw, 1956; Walther et al., 1995; Ague, 1991, 1994, 1997; Ferry, 1994; Penniston Dorland & Fery, 2008; Ague, 2014; Forshaw & Pattison, 2023). Nevertheless, the petrologic community at large mostly overlooks such aspects and follows the simplifying assumption that regional metamorphism is isochemical. The most recent and extensive bulk composition compilation of metapelites (Forshaw & Pattison, 2023) has shown that, apart from changes in volatile content and Fe^{3+}, regional metamorphism is indeed close to isochemical. However, relevant proportions of mineralized veins (predominantly of quartz) in the archetypal Barrovian sequence (Stonehaven, Scotland) and other Barrovian-style metamorphic terranes (e.g., vol% of quartz veins in each metamorphic terrane: Stonehaven, Scotland, 1-18%; Wepawaug Schist, Connecticut, 20-30%; Waits River Formation, Vermont, 4.5-12%; Otago Schist, New Zealand, up to 30%; Ague, 1994b; Breeding & Ague, 2002; Masters & Ague, 2005; Penniston-Dorlan & Ferry, 2008) indicate the occurrence of relevant mass transfer across orogenic wedges. An in-depth review of this topic is out of the scope of this work and the reader is referred to the chapter of Ague (2014) in the 2nd Edition of the Treatise on Geochemistry for further reading. In simplifying terms, multiple first-order physical, chemical and thermodynamic aspects have to be considered when dealing with fluid-mediated mass transfer across orogenic wedges. In a typical regionally metamorphosed terrain, prograde metamorphism continuously and progressively releases fluid. Such fluid can escape its source region by either porous flow or channelised flow (e.g., fractures, shear zones, lithologic contacts, permeable layers, fold hinges, and boudin necks; Ague, 2014; Tursi et al., 2018) both of which have multiple sub-variant that are a combination of these two endmembers. However, even if fluid is present and could escape the system, some chemical and thermodynamic conditions for elemental mobilization or precipitation necessarily must be met. This is embodied in the direction of the fluid flow, which can either be in a direction of increasing temperature (up-*T*) or decreasing temperature (down-*T*). Direction flow is fundamental because will create the chemical and thermodynamic conditions for fluid under- or over-saturation in rock-forming components, which will either result in rock dissolution or mineral precipitation. To show, in a simplified way, these concepts, the modelled SiO_2 solubility (i.e., silica saturation in the fluid) have been interpolated and overlayed over two simple numerical models for orogenic wedge where fluid production and flow are taken into account (Fig. 6; Lyubetskaya & Ague, 2009, 2010). The most common fluid direction is down-*T* during prograde metamorphism (Hanson, 1997; Lyubetskaya and Ague, 2009 and references therein): fluids will most likely either be at silica saturation or over-saturation conditions, resulting in

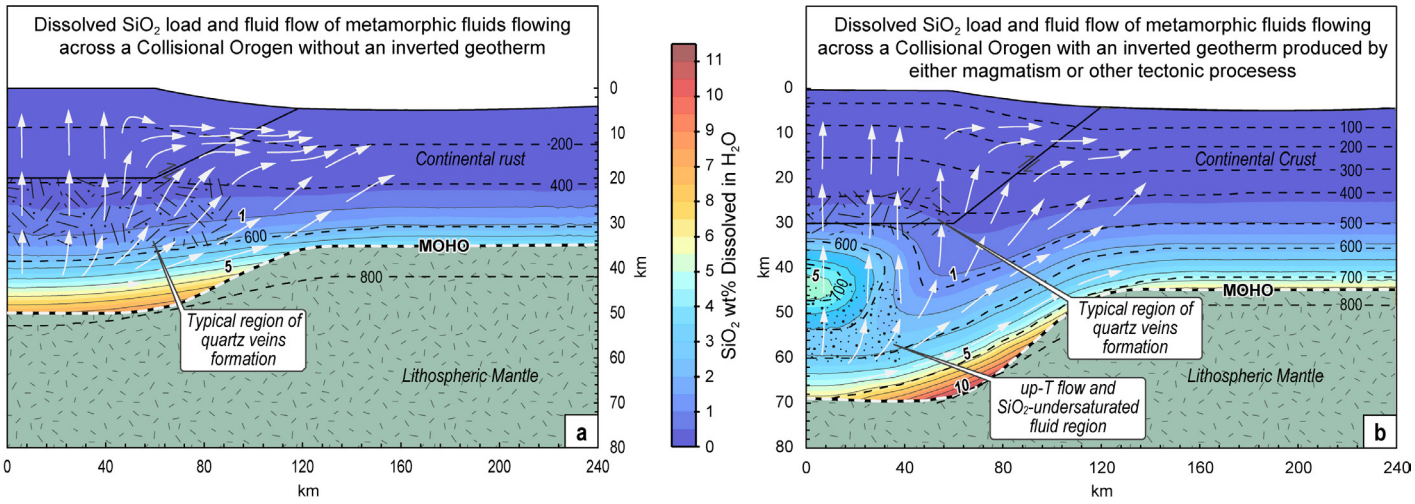

Fig. 6 - Silica saturation in aqueous fluids contoured over the thermal model for metamorphic fluid flow in collisional orogens from Lyubetskaya and Ague (2009): model with fluid production, exhumation rate of 1 mm/yr after 10 Myr. b) Silica saturation in aqueous fluids contoured over the thermal model for metamorphic fluid flow in collisional orogens with perturbed geothermal regime from Lyubetskaya and Ague (2010): model with fluid production, exhumation/erosion of 1 mm/yr after 6 Myr (from begging of the model) and magmatism at 5 Myr

marginal silica mobilization and redistribution through the crust (Fig. 6a). Conversely, up-*T* flow is necessary for relevant mass – silica – mobilization. This might be achieved at a regional scale by two scenarios: either by convective circulation from shallow to higher depths or where inverted geotherms are produced (Lyubetskaya & Ague, 2009, 2010 and references therein). The first scenario is limited to the brittle and colder portion of the crust (i.e., down to 15km of depths; Lyubetskaya & Ague, 2009) and as such is, as a matter of fact, unable to explain the observed volumes of quartz veins. The second scenario, however, results in upward fluid flow from lower T to higher *T* conditions that will result in silica–undersaturation in the fluid. Two ways exist to produce such perturbated geothermal regimes: (i) deep- to mid-crustal level intrusions with fluids flowing around the intrusions and (ii) long-lived under-thrusting can lead to inverted geotherms at the base of the over-thrusted plate and top of the under-thrusted plate (e.g., between the Main Central Thrust and the South Tibetan Detachment System, Himalaya; Cottle et al., 2015). In this scenario, fluid will rise through such thermal anomalies, dissolve silica (due to silica undersaturation in the fluid of roughly 2-3 wt% between 600°C at 60 km and 700°C at 45 km; Fig. 6b) and then precipitate it in veins and opening at shallower and colder depths (Fig. 6b). Thus mass transfer across orogenic wedges can occur only in regions of intense fluid flux where such fluids may find themselves undersaturated in rock-forming elements for the *P-T-X* conditions at which they will re-equilibrate.

CONCLUSIONS

Novel electrolytic fluid thermodynamic modelling based on recent advances in computational petrology (i.e., DEW model and lagged-speciation algorithm; Sversjenky et al., 2014; Galvez et al., 2015; Connolly & Galvez, 2018) allows modelling SiO_2 solubility in H_2O in a vast range of *P* and *T* conditions. What emerges is that, even though huge advancements have been made in the computational capability of complex fluids, some problems remain unresolved, like dealing with criticality and the continuous transition from supercritical fluids and hydrous melts. Experimentally determined silica solubilities are well reproduced up to 20 wt% of dissolved load (while being slightly underestimated by 1-10 wt% up to 50 wt%) and problems arise only around the *P-T* region where supercritical behaviour is expected. This calls for more experiments at supercritical conditions, especially on the high-pressure and high-temperature side of the critical point. The SiO_2-H_2O system is an exemplary chemical system for understanding how the chemical composition of fluids changes in a continuous way across vast *P-T* regions. It shows how mineral dissolution is a petrologic process capable of effective mass transfer at sub-arc depths (with fluids carrying between 5 wt% and > 70 wt% of dissolved silica) as well at shallower regional metamorphic conditions (with fluids capable of carrying up to 30 wt%). Moreover, its speciation allows visualising the increase in Si polymerisation (and thus fluid polymerisation) that is expected when an aqueous fluid evolves into a supercritical liquid, a transitional step before becoming a fully polymerised hydrous melt. Finally, the relevant silica solubility encountered both in experiments and in thermodynamic modelling, put into question the extent to which metamorphism can be considered isochemical and how common the conditions necessary for silica mobilisation in regional metamorphism can be encountered (Ague, 1991; Forshaw & Pattison, 2023), with superficial quartz vein being a potential by-product of silica mobilisation from the deeper portion of collisional orogens.

ACKNOWLEDGMENTS

I thank the insightful and constructive comments and reviews of Jacob Forshaw and an anonymous reviewer, which helped to clarify and expand a previous version of the manuscript. Alessandro Petroccia is thanked for providing the quartz-vein sample shown in Figure 1. The author also thanks the Editor in Chief Matteo Berti and the Associate Editor for the editorial handling of this manuscript.

REFERENCES

Ague J.J. (1991) - Evidence for major mass transfer and volume strain during regional metamorphism of pelites. Geology, 19(8), 855-858, https://doi.org/10.1130/0091-7613(1991)019<0855:EFMMTA>2.3.CO;2.

Ague J.J. (1994) - Mass transfer during Barrovian metamorphism of pelites, south-central Connecticut; I, Evidence for changes in composition and volume. American Journal of Science, 294(8), 989-1057, https://doi.org/10.2475/ajs.294.8.989.

Ague J.J. (1997) - Crustal mass transfer and index mineral growth in Barrow's garnet zone, northeast Scotland. Geology, 25(1), 73-76, https://doi.org/10.1130/0091-7613(1997)025<0073:CMTAIM>2.3.CO;2.

Ague J.J. (2014) - Fluid Flow in the Deep Crust, in: Treatise on Geochemistry: Second Edition. Elsevier Ltd., pp. 203-247, https://doi.org/10.1016/B978-0-08-095975-7.00306-5.

Anderson G.M. & Burnham C.W. (1965) - The solubility of quartz in super-critical water. American Journal of Science, 263(6), 494-511, https://doi.org/10.2475/ajs.263.6.494.

Breeding C.M. & Ague J.J. (2002) - Slab-derived fluids and quartz-vein formation in an accretionary prism, Otago Schist, New Zealand. Geology, 30(6), 499-502, https://doi.org/10.1130/0091-7613(2002)030<0499:SDFAQV>2.0.CO;2.

Connolly J.A. & Galvez M.E. (2018) - Electrolytic fluid speciation by Gibbs energy minimization and implications for subduction zone mass transfer. Earth Planet. Sc. Lett., 501, 90-102, https://doi.org/10.1016/j.epsl.2018.08.024.

Copley A. & Weller O. (2022) - The controls on the thermal evolution of continental mountain ranges. J. Metamorph. Geol., 40, 1235-1270, https://doi.org/10.1111/jmg.12664.

Cottle J.M., Larson K.P. & Kellett D.A. (2015) - How does the mid-crust accommodate deformation in large, hot collisional orogens? A review of recent research in the Himalayan orogen. Journal of Structural Geology, 78, 119-133, https://doi.org/10.1016/j.jsg.2015.06.008.

Dvir O., Pettke T., Fumagalli P. & Kessel R. (2011) - Fluids in the peridotite–water system up to 6 GPa and 800 °C: new experimental constrains on dehydration reactions. Contrib. Mineral. Petr., 161(6), 829-844, https://doi.org/10.1007/s00410-010-0567-2.

Ferrando S., Frezzotti M.L., Dallai L. & Compagnoni R. (2005) - Multiphase solid inclusions in UHP rocks (Su-Lu, China): Remnants of supercritical silicate-rich aqueous fluids released during continental subduction. Chem Geol, 223(1-3), 68-81, https://doi.org/10.1016/j.chemgeo.2005.01.029.

Ferrando S., Frezzotti M.L., Petrelli M. & Compagnoni R. (2009) - Metasomatism of continental crust during subduction: the UHP whiteschists from the Southern Dora-Maira Massif (Italian Western Alps). J. Metamorph. Geol., 27(9), 739-756, https://doi.org/10.1111/j.1525-1314.2009.00837.x.

Ferrando S., Groppo C., Frezzotti M.L., Castelli D. & Proyer A. (2017) - Dissolving dolomite in a stable UHP mineral assemblage: Evidence from Cal-Dol marbles of the Dora-Maira Massif (Italian Western Alps). Am. Mineral., 102(1), 42-60, https://doi.org/10.2138/am-2017-5761.

Ferrando S., Petrelli M. & Frezzotti M.L. (2019) - Gradual and selective trace-element enrichment in slab-released fluids at sub-arc depths. Sci. Rep., 9(1), 1-9, https://doi.org/10.1038/s41598-019-52755-9.

Ferry J.M. (1994) - Overview of the petrologic record of fluid flow during regional metamorphism in northern New England. American Journal of Science, 294(8), 905-988, https://doi.org/10.2475/ajs.294.8.905.

Forshaw J.B. & Pattison D.R.M. (2023) - Major-element geochemistry of pelites: Geology, 5(1), 49-53, https://doi.org/10.1130/G50542.1.

Frezzotti M.L. (2019) - Diamond growth from organic compounds in hydrous fluids deep within the Earth. Nat. Commun., 10, 4952, https://doi.org/10.1038/s41467-019-12984-y.

Frezzotti M.L. & Ferrando S. (2015) - The chemical behaviour of fluids released during deep subduction based on fluid inclusions. Am Mineral, 100(2-3), 352-377, https://doi.org/10.2138/am-2015-4933.

Frezzotti M.L., Ferrando S., Dallai L. & Compagnoni R. (2007) - Intermediate alkali–alumino-silicate aqueous solutions released by deeply subducted continental crust: Fluid evolution in UHP OH-rich topaz–kyanite quartzites from Donghai (Sulu, China). J Petrol., 48(6), 1219-1241, https://doi.org/10.1093/petrology/egm015.

Frezzotti M.L., Selverstone J., Sharp Z.D. & Compagnoni R. (2011) - Carbonate dissolution during subduction revealed by diamond-bearing rocks from the Alps. Nature Geosci., 4, 703-706, https://doi.org/10.1038/ngeo1246.

Galvez M.E., Manning C.E., Connolly J.A. & Rumble D. (2015) - The solubility of rocks in metamorphic fluids: A model for rock-dominated conditions to upper mantle pressure and temperature. Earth Planet. Sc. Lett., 430, 486-498, https://doi.org/10.1016/j.epsl.2015.06.019.

Goncalves P., Oliot E., Marquer D. & Connolly J.A.D. (2012) - Role of chemical processes on shear zone formation: an example from the Grimsel metagranodiorite (Aar massif, Central Alps). J. Metamorph. Geol., 30(7), 703-722, https://doi.org/10.1111/j.1525-1314.2012.00991.x

Groppo C., Rolfo F. & Indares A. (2012) - Partial melting in the Higher Himalayan Crystallines of Eastern Nepal: the effect of decompression and implications for the 'Channel Flow' model. J. Petrol., 53(5), 1057-1088, https://doi.org/10.1093/petrology/egs009

Groppo C., Rolfo F. & Frezzotti M.L. (2022) - CO_2 outgassing during collisional orogeny is facilitated by the generation of immiscible fluids. Commun Earth Environ., 3, 13 (2022). https://doi.org/10.1038/s43247-022-00340-w.

Hack A.C., Hermann J. & Mavrogenes J.A. (2007) - Mineral solubility and hydrous melting relations in the deep earth: Analysis of some binary A–H_2O system pressure-temperature-composition topologies. Am. J. Sci., 307(5), 833-855, https://doi.org/10.2475/05.2007.03.

Hanson R.B. (1997) - Hydrodynamics of regional metamorphism due to continental collision. Economic Geology, 92(7-8), 880-891, https://doi.org/10.2113/gsecongeo.92.7-8.880.

Holland T.J.B. & Powell R. (2011) - An improved and extended internally consistent thermodynamic dataset for phases of petrological interest, involving a new equation of state for solids. J. Metamorph. Geol., 29(3), 333-383, https://doi.org/10.1111/j.1525-1314.2010.00923.x.

Holland T.J., Green E.C. & Powell R. (2018) - Melting of peridotites through to granites: a simple thermodynamic model in the system KNCFMASHTOCr. J. Petrol., 59(5), 881-900. https://doi.org/10.1093/petrology/egy048.

Huang F. & Sverjensky D.A. (2019) - Extended Deep Earth Water Model for predicting major element mantle metasomatism. Geochim. et Cosmochim. Ac., 254, 192-230, https://doi.org/10.1016/j.gca.2019.03.027.

Hunt J.D. & Manning C.E. (2012) - A thermodynamic model for the system SiO2–H2O near the upper critical end point based on quartz solubility experiments at 500–1100 C and 5–20 kbar. Geochim et Cosmochim Ac, 86, 196-213, https://doi.org/10.1016/j.gca.2012.03.006.

Kennedy G.C., Wasserburg G.J., Heard H.C. & Newton R.C. (1962) - The upper three-phase region in the system SiO_2-H_2O. Am. J. Sci., 260(7), 501-521, https://doi.org/10.2475/ajs.260.7.501.

Kessel R., Schmidt M.W., Ulmer P. & Pettke T. (2005) - Trace element signature of subduction-zone fluids, melts and supercritical liquids at 120–180 km depth. Nature, 437(7059), 724-727, https://doi.org/10.1038/nature03971.

Li Y. (2017) - Immiscible CHO fluids formed at subduction zone conditions. Geochem. Perspect. Lett., 3, 12-21, https://doi.org/10.7185/geochemlet.1702.

Lyubetskaya T. & Ague J.J. (2009) - Modeling the magnitudes and directions of regional metamorphic fluid flow in collisional orogens. Journal of Petrology, 50(8), 1505-1531, https://doi.org/10.1093/petrology/egp100.

Lyubetskaya T. & Ague J.J. (2010) - Modeling metamorphism in collisional orogens intruded by magmas: II. Fluid flow and implications for Barrovian and Buchan metamorphism, Scotland. American Journal of Science, 310(6), 459-491, https://doi.org/10.2475/06.2010.02.

Maffeis A., Ferrando S., Connolly J.A., Groppo C., Frezzotti M.L. & Castelli D. (2021) - Thermodynamic analysis of HP-UHP fluid inclusions: The solute load and chemistry of metamorphic fluids. Geochim. et Cosmochim. Ac., 315, 207-229, https://doi.org/10.1016/j.gca.2021.08.044.

Makhluf A.R., Newton R.C. & Manning C.E. (2016) - Hydrous albite magmas at lower crustal pressure: new results on liquidus H_2O content, solubility, and H_2O activity in the system $NaAlSi_3O_8$–H_2O–NaCl at 1.0 GPa. Contrib. Mineral. Petrol., 171, 75, https://doi.org/10.1007/s00410-016-1286-0.

Malaspina N., Hermann J., Scambelluri M. & Compagnoni R. (2006) - Polyphase inclusions in garnet–orthopyroxenite (Dabie Shan, China) as monitors for metasomatism and fluid-related trace element transfer in subduction zone peridotite. Earth Planet. Sc. Lett., 249(3-4), 173-187, https://doi.org/10.1016/j.epsl.2006.07.017.

Manning C.E. (1994) - The solubility of quartz in H_2O in the lower crust and upper mantle. Geochim et Cosmochim Ac, 58(22), 4831-4839, https://doi.org/10.1016/0016-7037(94)90214-3.

Manning C.E. (2004a) - The chemistry of subduction-zone fluids. Earth Planet. Sc. Lett., 223(1-2), 1-16, https://doi.org/10.1016/j.epsl.2004.04.030.

Manning C.E. (2004b) - Polymeric silicate complexing in aqueous fluids at high pressure and temperature, and its implications for water-rock interaction, in Wanty, R. B., and Seal, R. R., II, eds., Water-Rock Interaction, Proceedings of the Eleventh International Symposium on Water-Rock Interaction. London, Taylor & Francis Group, p. 45-49

Manning C.E. (2018) - Fluids of the Lower Crust: Deep Is Different. Annu. Rev. Earth Planet. Sci., 46, 67-97, https://doi.org/10.1146/annurev-earth-060614-105224.

Manning C.E. & Frezzotti M.L. (2020) - Subduction-zone fluids. Elements (2020) 16(6), 395-400, https://doi.org/10.2138/gselements.16.6.395.

Masters R.L. & Ague J.J. (2005) - Regional-scale fluid flow and element mobility in Barrow's metamorphic zones, Stonehaven, Scotland. Contributions to Mineralogy and Petrology, 150, 1-18, https://doi.org/10.1007/s00410-005-0005-z.

Mysen B.O. (2010) - Speciation and mixing behavior of silica-saturated aqueous fluid at high temperature and pressure. American Mineralogist, 95(11-12), 1807-1816. https://doi.org/10.2138/am.2010.3539.

Mysen B.O. (2012) - Silicate-COH melt and fluid structure, their physicochemical properties, and partitioning of nominally refractory oxides between melts and fluids. Lithos, 148, 228-246, https://doi.org/10.1016/j.lithos.2012.06.005.

Newton R.C. & Manning C.E. (2003) - Activity coefficient and polymerization of aqueous silica at 800 C, 12 kbar, from solubility measurements on SiO_2-buffering mineral assemblages. Contrib. Mineral. Petrol. 146, 135-143, https://doi.org/10.1007/s00410-003-0483-9.

Newton R.C. & Manning C.E. (2008) - Solubility of corundum in the system Al_2O_3–SiO_2–H_2O–NaCl at 800° C and 10 kbar. Chem. Geol., 249(3-4), 250-261, https://doi.org/10.1016/j.chemgeo.2008.01.002.

Penniston-Dorland S.C. & Ferry J.M. (2008) - Element mobility and scale of mass transport in the formation of quartz veins during regional metamorphism of the Waits River Formation, east-central Vermont. American Mineralogist, 93(1), 7-21, https://doi.org/10.2138/am.2008.2461.

Philippot P., Chevallier P., Chopin C. & Dubessy J. (1995) - Fluid composition and evolution in coesite-bearing rocks (Dora-Maira massif, Western Alps): implications for element recycling during subduction. Contrib. Mineral. Petrol., 121, 29, https://doi.org/10.1007/s004100050088.

Pitzer K.S. & Sterner S.M. (1994) - Equations of state valid continuously from zero to extreme pressures for H_2O and CO_2. J. Chem. Phys., 101, 3111, https://doi.org/10.1063/1.467624.

Ricci J.E. (1951) - The phase rule and heterogeneous equilibrium: New York, D. Van Nostrand Company.

Sanchez-Valle C. (2013) - Structure and thermodynamics of subduction zone fluids from spectroscopic studies. Rev Mineral Geochem, 76(1), 265-309, https://doi.org/10.1515/9781501508295-008.

Scambelluri M. & Philippot P. (2001) - Deep fluids in subduction zones. Lithos, 55(1-4), 213-227. https://doi.org/10.1016/S0024-4937(00)00046-3.

Schmidt M.W., Vielzeuf D. & Auzanneau E. (2004) - Melting and dissolution of subducting crust at high pressures: the key role of white mica. Earth Planet. Sc. Lett., 228(1-2), 65-84. https://doi.org/10.1016/j.epsl.2004.09.020.

Selverstone J., Franz G., Thomas S. & Getty S. (1992) - Fluid variability in 2 GPa eclogites as an indicator of fluid behavior during subduction. Contr. Mineral. and Petrol., 112, 341-357, https://doi.org/10.1007/BF00310465.

Shaw D. (1956) - Geochemistry of pelitic rocks. Part III: Major elements and general geochemistry. Bulletin of the Geological Society of America 67, 919-934, https://doi.org/https://doi.org/10.1130/0016-7606(1956)67[919:GOPRPI]2.0.CO;2.

Spandler C. & Pirard C. (2013) - Element recycling from subducting slabs to arc crust: A review. Lithos, 170, 208-223, https://doi.org/10.1016/j.lithos.2013.02.016.

Steele-MacInnis M. & Manning C.E. (2020) - Hydrothermal properties of geologic fluids. Elements., 16(6), 375-380, https://doi.org/10.2138/gselements.16.6.375.

Sverjensky D.A. (1987) - Calculation of the thermodynamic properties of aqueous species and the solubilities of minerals in supercritical electrolyte solutions Rev. Mineral. Geochem., 17(1), 177-209.

Sverjensky D.A. (2019) - Thermodynamic modelling of fluids from surficial to mantle conditions. J. Geol. Soc. London, 176(2), 348-374, https://doi.org/10.1144/jgs2018-105.

Sverjensky D.A., Harrison B. & Azzolini D. (2014) - Water in the deep Earth: the dielectric constant and the solubilities of quartz and corundum to 60 kb and 1200° C. Geochim. et Cosmochim. Ac., 129, 125-145, https://doi.org/10.1016/j.gca.2013.12.019.

Syracuse E.M., van Keken P.E. & Abers G.A. (2010) - The global range of subduction zone thermal models. Phys. Earth Planet. In., 183(1-2), 73-90, https://doi.org/10.1016/j.pepi.2010.02.004.

Thompson A. B. (2010) - Perspectives on metamorphic processes and fluids. Elements, 6(3), 142-143.

Touret J.L., Frezzotti M.L., Carswell D.A. & Compagnoni R. (2003) - Fluid inclusions in high pressure and ultrahigh pressure metamorphic rocks. In Ultrahigh pressure metamorphism, 5, 467-487. Eötvös University Press Budapest.

Tursi F. (2022) - The key role of μH2O gradients in deciphering microstructures and mineral assemblages of mylonites: examples from the Calabria polymetamorphic terrane. Miner. Petrol., 116, 1-14, https://doi.org/10.1007/s00710-021-00766-8.

Tursi F., Festa V., Fornelli A., Micheletti F. & Spiess R. (2018) - Syn-shearing mobility of major elements in ductile shear zones: state of the art for felsic deformed protoliths. Periodico di Mineralogia, 87(3), https://dopi.org/10.2451/2018PM811.

Walther J.V., Holdaway M.J. & Ague J.J. (1995) - Mass transfer during Barrovian metamorphism; discussion and reply. Am. J. Sci., 295, 1020-1033, https://doi.org/doi.org/10.2475/ajs.295.8.1020.

Wang H.M., Henderson G.S. & Brenan J.M. (2004) - Measuring quartz solubility by in situ weight-loss determination using a hydrothermal diamond cell. Geochim. et Cosmochim. Ac., 68(24), 5197-5204, https://doi.org/10.1016/j.gca.2004.06.006.

White R.W., Powell R., Holland T.J.B., Johnson T.E. & Green E.C.R. (2014) - New mineral activity–composition relations for thermodynamic calculations in metapelitic systems. Journal of Metamorphic Geology, 32(3), 261-286, https://doi.org/10.1111/jmg.12071.

Yardley B.W.D. & Graham J.T. (2002) - The origins of salinity in metamorphic fluids. Geofluids, 2(4), 249-256, https://doi.org/10.1046/j.1468-8123.2002.00042.x.

Yardley B.W.D. & Bodnar R.J. (2014) - Crustal fluid compositions: the basics. Fluids in the Continental Crust, 127.

Zotov N. & Keppler H. (2002) - Silica speciation in aqueous fluids at high pressures and high temperatures. Chem. Geol., 184(1-2), 71-82, https://doi.org/10.1016/S0009-2541(01)00353-9.